Nanotechnology **21** (2010) 305701 (10pp) doi:10.1088/0957-4484/21/30/305701

Characterization of silver–gallium nanowires for force and mass sensing applications

Laura B Biedermann[1,5,6], Ryan C Tung[2], Arvind Raman[2], Ronald G Reifenberger[1], Mehdi M Yazdanpanah[3,4] and Robert W Cohn[3]

[1] Department of Physics and Birck Nanotechnology Center, Purdue University, W. Lafayette, IN 47907, USA
[2] School of Mechanical Engineering and Birck Nanotechnology Center, Purdue University, W. Lafayette, IN 47907, USA
[3] ElectroOptics Research Institute and Nanotechnology Center, University of Louisville, Louisville, KY, USA
[4] NaugaNeedles LLC, Louisville, KY, USA

E-mail: lbieder@sandia.gov

Received 10 April 2010, in final form 21 May 2010
Published 6 July 2010
Online at stacks.iop.org/Nano/21/305701

Abstract
We investigate the mechanical properties of cantilevered silver–gallium (Ag_2Ga) nanowires using laser Doppler vibrometry. From measurements of the resonant frequencies and associated operating deflection shapes, we demonstrate that these Ag_2Ga nanowires behave as ideal Euler–Bernoulli beams. Furthermore, radial asymmetries in these nanowires are detected through high resolution measurements of the vibration spectra. These crystalline nanowires possess many ideal characteristics for nanoscale force and mass sensing, including small spring constants (as low as 10^{-4} N m^{-1}), high frequency bandwidth with resonance frequencies in the 0.02–10 MHz range, small suspended mass (picograms), and relatively high Q-factors (∼2–50) under ambient conditions. We evaluate the utility of Ag_2Ga nanowires for nanocantilever applications, including ultrasmall mass and high frequency bandwidth piconewton force detection.

S Online supplementary data available from stacks.iop.org/Nano/21/305701/mmedia

(Some figures in this article are in colour only in the electronic version)

1. Introduction

The advantages of micro and nanomechanical cantilevers as versatile, label-free sensors of gas, chemical or biological entities are now well established [1–6]. In the mass sensing modality, the added mass of the analyte is usually transduced as a resonance frequency shift of the micro/nanocantilever sensor. For such sensors, the minimum detectable added mass scales with the mass of the cantilever and inversely with its quality factor [7]. The current trend in mass detection in ultra high vacuum environments is pushing past femtogram sensitivity toward zeptogram mass sensing [8] for single molecule detection and eventually towards mass spectroscopy [9]. To achieve such high mass resolution requires decreasing the effective mass of the cantilever by reducing its size while simultaneously maintaining a high Q-factor [10, 11]. However, the use of ultrasmall cantilever technology comes with its own challenges including, for instance, the need for sensitive, low noise piezoelectric, piezoresistive, or magnetomotive transduction of vibration and high frequency electronics to monitor the vibration of such cantilevers. Thus there is significant interest in the

[5] Present address: Sandia National Laboratories, Albuquerque, NM, USA.
[6] Author to whom any correspondence should be addressed.

development of ultrasmall cantilever technology with standard transduction to measure its vibrations. For this reason we investigate a high resolution optical transduction technique to measure the thermal and driven resonances of reflective silver–gallium (Ag_2Ga) nanowires.

Cantilevered Ag_2Ga nanowires have recently gained interest for various scanning probe microscopy applications [12] since they are robust, conductive, nearly cylindrical nanowires with a high aspect ratio that can be fabricated on a variety of surfaces. As we will show in this paper, their vibrations can be easily measured *optically* using commercially available laser Doppler vibrometry (LDV). Since the dimension and location of individual Ag_2Ga nanowires can be well controlled, Ag_2Ga nanowires are promising candidates for use as nanocantilevers in novel mass sensing and force transducing applications.

Previously, the elastic modulus (E) of a set of Ag_2Ga nanowires was determined from measurements of their driven response near resonance [13], as observed using a scanning electron microscope (SEM) using techniques similar to those employed elsewhere to measure the resonant response of driven multiwalled carbon nanotubes (MWNTs) [14]. From the measured resonance frequencies and dimensions of the Ag_2Ga nanowires, E was estimated to be 42.6 ± 22.4 GPa. Uncertainty in the measurements of the nanowires' dimensions accounted for the large margin of error. For a subset of seven nanowires, Q-factors of 600–3300 in vacuum were estimated from the 3 dB-point of the driven resonance peak [13]. However the eigenmodes of these nanocantilevers were not measured, and observing the oscillation amplitude as a function of drive frequency in an SEM is not a suitable method for accurately estimating the Q-factor. In a force transduction application, [15, 16] the buckled shape of a long Ag_2Ga nanowire was measured to determine the applied *static* force. Applications to the sensing of time-varying forces were not considered.

In what follows, we describe optical measurements of the vibrations of Ag_2Ga nanowires, including higher order vibrations, and investigate cross-sectional asymmetry and the effect of air damping. We show that Ag_2Ga nanocantilevers have high resonant frequencies, Q-factors of 2–50 under ambient conditions, and effective masses that are 3–5 orders of magnitude smaller than conventional microcantilevers. These characteristics render Ag_2Ga nanocantilevers as a promising platform for ultrasmall mass sensing and high sensitivity, high bandwidth force sensing; potential applications for Ag_2Ga nanowires include acoustic sensing, atomic force microscopy (AFM), and accelerometry.

This paper is organized as follows. First, an overview of Ag_2Ga nanowire fabrication and the capabilities of the LDV system are presented. A brief theoretical discussion of the expected eigenfrequencies and power spectral density of the thermal response of the nanocantilevers follows. This theoretical discussion is supported by the measured thermal vibration spectra and driven eigenmodes of representative Ag_2Ga nanowires under ambient and vacuum conditions. To conclude, we discuss the force sensitivity and bandwidth of Ag_2Ga nanowires and compare the quality factors and mass sensing capabilities of Ag_2Ga nanocantilevers with those of other resonators such as MWNTs and Si microcantilevers.

2. Experimental considerations

2.1. Fabrication of Ag_2Ga nanowires

Yazdanpanah *et al* developed a unique nanofabrication method to grow individual Ag_2Ga nanowires at designated locations and orientations on various surfaces. These surfaces are prepared by sputter coating first a 10 nm Cr adhesion layer followed by a 100 nm Ag layer [12, 13, 17]. The sputtered Ag provides the material for nanowire growth. Nanomanipulators inside an SEM allow these coated surfaces to be dipped into a sphere of liquid Ga resting on a silicon substrate. As the surface is retracted, Ag_2Ga crystallizes, forming individual nanowires with lengths much greater than the thickness of the Ga meniscus. The length and diameter of the nanowire depends on the thickness of the Ag layer and the rate at which the surface is withdrawn. These nanowires can be controllably fabricated with diameters of 25–500 nm and lengths of 1–110 μm. Typically the Ag_2Ga nanowires are fabricated on sharp protruding surfaces such as those at the end of etched tungsten wires or on the tip of AFM cantilevers.

X-ray diffraction patterns and transmission electron microscope (TEM) micrographs show that the Ag_2Ga nanowires are crystalline, hexagonal closed pack (HCP) structures, with 8–16 facets forming a nearly-circular cross-section and uniform diameter along their length [12, 17]. Based on the stoichiometric ratio, the density of the Ag_2Ga nanowires is estimated to be 8960 kg m^{-3} [17].

Eight Ag_2Ga nanowires with diameters from 65 to 300 nm and lengths from 4 to 60 μm were prepared to systematically investigate their mechanical properties using the LDV. Using a Zeiss Supra 35 SEM, SEM characterization of each Ag_2Ga nanowire was performed in advance. The nanowires studied, which are representative of the typical range of lengths and diameters available using this nanofabrication method, are listed in table 1. These nanowires were grown on both etched tungsten tips and conventional AFM cantilevers[7]. No characteristic difference was observed for the nanowires grown on tungsten tips versus AFM cantilever tips.

2.2. LDV measurements of elastic modulus, Q-factor, and bending stiffness of Ag_2Ga nanowires

The thermally-driven vibration spectra of an individual Ag_2Ga nanowire are recorded using a Polytec MSA-400 scanning LDV that is located on a 30 000 kg cement slab supported by six air spring dampers to reduce floor vibrations. The same system had been previously used by the authors to study the vibration of MWNTs [18]; a similar system was recently used by Nakayama *et al* to measure the vibrations of metallic glassy nanowires [19]. The vibrometer measures velocities in the frequency range from 0 to 1.5 MHz and displacements in the range from 0.050 to 20 MHz. The frequency resolution of the LDV is inversely proportional to the sample acquisition time; while resolutions of 1 Hz are possible, the data reported in this manuscript were typically acquired with resolutions of 100 Hz. A detailed discussion of the optical pathway for the LDV can be found in [20].

[7] Vistaprobes T300 tapping mode silicon probes from Nanoscience Instruments with nominal $k_c = 40$ N m^{-1} and $f_1 = 300$ kHz were used.

Table 1. Dimensions of the eight Ag_2Ga nanowires studied in this work. Nanowires NW2, NW4, NW5, and NW8 are discussed in more detail in the text.

Designation	Length (μm)	Diameter (nm)	Notable characteristic
NW1	23 & 30	115 & 194	Two conjoined nanowires of unequal diameter and length
NW2	60	206	Long, straight nanowire
NW3	9.6	163	Short, stiff nanowire
NW4	4.3	96	Large frequency bandwidth (2 MHz)
NW5	6.2	106	Large frequency bandwidth (1 MHz)
NW6	22	65	Very soft nanocantilever (spring constant $\sim 10^{-5}$ N m^{-1})
NW7	10	301	High Q-factor (50) at ambient pressure
NW8	16.6 & 17	140	Two conjoined nanowires of nearly equal diameter and length

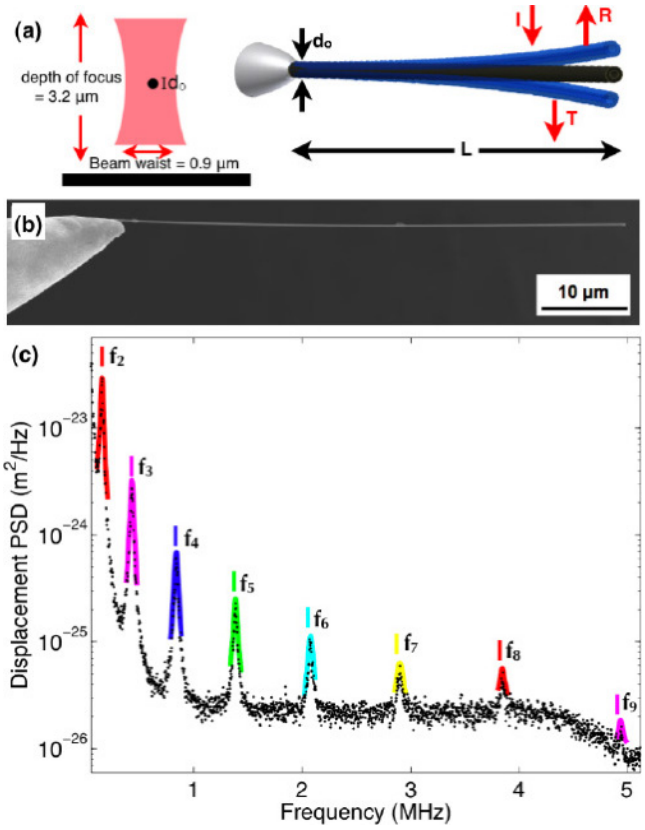

Figure 1. In (a), schematics of laser light focused on a nanowire and of a nanowire mounted on a tip. A portion of the incident light, I, is reflected, R, off of the nanowire, allowing transverse vibrations to be detected. In (b), an SEM micrograph of NW2, which was grown on a Ag-coated tungsten tip. In (c), the measured displacement PSD of thermally-excited NW2 clearly reveals the 2nd through 9th eigenfrequencies. The tick marks above the spectra peaks indicate the expected theoretical location of each eigenfrequency peak using equation (2). In (c), overlaid least square curve fits to equation (5) indicate the frequency range used to calculate Q_j, f_j, and $\langle z_j^2 \rangle$.

To measure the vibration spectrum, the LDV collects light backscattered from a laser beam focused onto a single Ag_2Ga nanowire, as indicated in figure 1(a). Due to the high reflectance of the nanowires, all of the nanowires studied could be readily observed in the optical microscope of the LDV. The incident beam of the interferometer (diameter 0.9 μm, wavelength λ =633 nm, power $<$ 1 mW) is focused through a 50$\times$ microscope objective and is incident normal to the oscillating Ag_2Ga nanowire. The backscattered light is recombined with a reference beam and the nanowire's transverse bending displacement is detected by counting the interference fringes. The nanowire's velocity is determined from the Doppler shift of the backscattered light [18, 20]. The nanowire vibration spectra were primarily measured using a displacement decoder so that higher eigenfrequencies ($>$1.5 MHz) could be detected. A key advantage of the LDV technique is the ability to measure the eigenmodes of the nanowire by scanning the beam along the nanowire's length. When operating in this mode, the nanowire is mounted on top of a piezoelectric transducer and driven near its resonance frequencies using a driven excitation mode of the LDV.[8] With the phase information obtained from the drive signal, the operating deflection shape (ODS) of the nanowire can be inferred. For structures with widely spaced resonances with reasonably high Q-factors, as in this study, the ODS is equivalent to the eigenmode.

To study the vibrational properties of the Ag_2Ga nanowires at low pressures, the LDV was fitted with a simple stainless steel vacuum chamber having a Kodial glass viewport that could be pumped to pressures less than 1 Torr. In order to accurately resolve the sharper eigenfrequency peaks, the displacement spectrum at such low pressures was measured with a higher frequency resolution.

3. Thermal vibration response of Ag_2Ga nanocantilevers: theoretical considerations

Before presenting the experimental results, we discuss the theoretical thermal vibration spectra expected of such cantilevered structures. The expected vibrational spectra of a Ag_2Ga nanowire can be modeled by treating the nanowire as a cantilevered beam of length L and uniform cross-sectional area A. The transverse eigenfrequencies, ω_j, of oscillation for a cantilevered beam are given by Euler–Bernoulli beam theory

$$\omega_j = \frac{\alpha_j^2}{L^2}\sqrt{\frac{EI}{\rho A}}, \tag{1}$$

where E is the elastic modulus, I is the areal moment, ρ is the density of the nanowire, and α_1 =1.875, α_2 = 4.694$\cdots$ [21]. The integer subscripts $j = 1, 2, \ldots$ correspond

[8] To excite the driven resonances of the nanowire, the 'pseudo random' excitation mode of the Polytec LDV is used. In this mode, the piezoelectric transducer is simultaneously excited by 6400 sinusoidal signals of equal magnitude in the specified frequency range, 0 Hz to f_{max}.

Table 2. The measured eigenfrequencies $f_j = \omega_j/(2\pi)$, quality factors, mean square displacements, modal stiffnesses, and elastic moduli from the 1st–9th eigenmodes of NW2. The first eigenfrequency was measured using the velocity decoder (*); the second through ninth eigenfrequencies were measured using the displacement decoder.

j	f_j (MHz)	Q_j	$\langle z_j^2 \rangle$ (nm^2)	$k_{j,\mathrm{thermal}}$(N m^{-1})	$k_{j,\mathrm{mat}}$(N m^{-1})	E (GPa)
1*	0.0256	2.2	32	1.27×10^{-4}	1.2×10^{-4}	93.1
2	0.152	5.0	0.84	0.0048	0.0042	83.2
3	0.428	13	0.10	0.041	0.032	84.5
4	0.838	21	0.024	0.17	0.12	84.4
5	1.388	34	0.0098	0.41	0.34	84.7
6	2.079	35	0.0054	0.75	0.76	85.2
7	2.900	34	0.0036	1.1	1.5	85.0
8	3.846	65	0.0032	1.3	2.6	84.3
9	4.938	100	0.0011	3.8	4.3	84.2

to the first, second, and higher transverse eigenmodes. While the nanowires are multifaceted, their cross-section is approximately circular; in this case, $I = \pi d^4/64$, and equation (1) simplifies to

$$\omega_j = \frac{\alpha_j^2}{4L^2} d \sqrt{\frac{E}{\rho}}, \tag{2}$$

where d is the diameter of the nanowire. Thus the vibration spectrum from a cantilevered nanowire should contain a sequence of sharp peaks corresponding to the eigenfrequencies ω_j given above. For nanowires of the dimensions in table 1, estimates for the ω_1 range from tens of kilohertz for the longest nanowires to several megahertz for the shortest nanowires.

These eigenfrequencies and associated Q-factors can be identified from the measured power spectral density (PSD) of thermally-excited Ag_2Ga nanowires. The fluctuation-dissipation theorem relates the equilibrium thermal fluctuations of an object to its dissipation in the surrounding medium. For the case of a classical oscillator, the fluctuation-dissipation theorem states that [22]

$$S_{zz}(\omega) = \frac{2k_\mathrm{B}T}{\omega} \mathrm{Im}\{Z(\omega)\}, \tag{3}$$

where $S_{zz}(\omega)$ is the PSD of the oscillation, k_B is Boltzmann's constant, T is temperature, ω is the frequency, and $Z(\omega)$ is the frequency response function (FRF) relating the nanowire deflection to applied force.

The FRF $Z_j(\omega)$ for each eigenmode ($j = 1, 2, \ldots$) of the Ag_2Ga nanocantilever can be written as

$$Z_j(\omega_j) = \frac{1}{k_j[1 - (\frac{\omega}{\omega_j})^2 + \mathrm{i}\frac{\omega}{Q_j\omega_j}]}, \tag{4}$$

where k_j is the modal bending stiffness of the nanocantilever and Q_j is the Q-factor of the jth eigenmode. Accordingly, the overall PSD of the transverse thermal vibration of the nanocantilever is expected to be composed of the thermal response of the individual eigenmodes and can be written as:

$$S_{zz,j}(\omega) = \sum_{j=1}^{\infty} \frac{2k_\mathrm{B}T}{m\omega_j^3 Q_j} \frac{1}{[1 - (\frac{\omega}{\omega_j})^2]^2 + (\frac{\omega}{Q_j\omega_j})^2}, \tag{5}$$

where $m \approx 0.254\rho AL$ is the suspended mass of the nanowire. The expression given above in equation (5) is useful to extract the Q-factors and natural frequencies

$$S_{zz,j}(\omega) = \frac{A_j}{Q_j\omega_j^3} \frac{\omega^2}{[1 - (\frac{\omega}{\omega_j})^2]^2 + (\frac{\omega}{Q_j\omega_j})^2} + \mathrm{Noise}_j. \tag{6}$$

where Noise_j refers to the noise floor encountered in the PSD near the jth peak of the eigenmode and the additional ω^2 term is introduced in the numerator to account for this being a velocity spectrum.

4. Vibrational spectra of cantilevered Ag_2Ga nanowires

The thermal vibrational spectra of eight Ag_2Ga nanowires were measured using the LDV. In what follows, the vibration spectra of four representative Ag_2Ga nanowires, NW2, NW4, NW5, and NW8, are discussed in detail.

4.1. Eigenfrequencies and modal stiffnesses of a long Ag_2Ga nanowire

The thermal vibration spectra of an exceptionally long nanowire, NW2, ($L = 60\ \mu$m, $d = 205.5$ nm) were measured using both the velocity and the displacement decoders. Both decoders were used since the first eigenfrequency (near $f_1 = 0.026$ MHz) was below the frequency limit (0.050 MHz) of the displacement decoder. Figure 1(b) shows an SEM micrograph of nanowire NW2 while figure 1(c) plots the measured thermal displacement spectrum of the same Ag_2Ga nanowire. Each peak in the displacement spectra is fit by an equation of the form given in equation (5); these overlaid curve fits are also provided in figure 1(c). From these fits, the ω_j and associated Q_j were accurately determined. Table 2 tabulates the measured eigenfrequencies, Q-factors, and mean square displacements (MSD), $\langle z_j^2 \rangle$, as well as the calculated modal stiffness and elastic modulus for the 1st–9th eigenmodes of NW2.[9]

The eigenfrequency peaks were readily identified by comparing the measured ratio of frequencies $\omega_1{:}\omega_2{:}\omega_3{:}\cdots$ to

[9] The values in table 2 are calculated as follows. f_j and Q_j are determined by curve fits to equations (5) ($j = 1$) and (6) ($j > 1$). Numerical integration of the area under each curve yields $\langle z_j^2 \rangle$. Assuming a room temperature of 293 K, $k_{j,\mathrm{thermal}}$ is calculated from equation (8). E is calculated from equation (7); this value of E is used to calculate $k_{j,\mathrm{mat}}$ following equation (9).

those predicted from theory $\alpha_1^2{:}\alpha_2^2{:}\alpha_3^2{:}\cdots$ (see equation (2)). From this comparison, the spectra peaks were identified as corresponding to the 2nd through 9th eigenmodes for the displacement spectrum (see table 2) and the 1st through 4th eigenmodes of vibration for the velocity spectrum (see table 4). A small discrepancy (less than 1%) in the experimentally determined frequency ratios demonstrates that the motion of this straight, high-aspect ratio nanowire is well described by Euler–Bernoulli beam theory.

From the measured ω_j and the dimensions of NW2, E is calculated by inverting equation (2):

$$E = \left\langle \frac{16\rho}{\alpha_j^4 d^2}\omega_j^2 L^4 \right\rangle. \tag{7}$$

In this way, an accurate estimate for the elastic modulus for NW2 was found to be $E = 84.4 \pm 0.6$ GPa, where the error in the measurement is due to the variance in the eight measured f_2–f_9.

The LDV technique offers two independent methods to calculate the modal stiffness, k_j, based on either the thermal motion or the material properties. First, by the equipartition theorem, $k_{j,\text{thermal}}$ is calculated for each eigenmode as follows [21]:

$$\tfrac{1}{2}k_b T = \tfrac{1}{2}k_{j,\text{thermal}}\langle z_j^2\rangle. \tag{8}$$

The thermally-driven MSD, $\langle z_j^2\rangle$, is calculated by numerically integrating the area of each eigenfrequency peak, as indicated by the curve fits in figure 1(c). The $k_{j,\text{thermal}}$ are calculated for a standard lab temperature of 293 K and are tabulated in table 2. Secondly, the modal stiffness can also be calculated from the known nanowire dimensions and E as follows [23]:

$$k_{j,\text{mat}} = k_c\alpha_j^4/12 \qquad \text{where } k_c = 3EI/L^3. \tag{9}$$

Knowing E, the static bending coefficient is $k_c = 1.02 \times 10^{-4}$ N m^{-1} for this nanowire. As tabulated in table 2, these two independent methods of calculating k_j are in good agreement.

We note in table 2 that the first measured eigenfrequency, $f_1 = 0.0256$ MHz, is higher by 4.8% than the value expected from Euler–Bernoulli beam theory. Subsequent experiments showed that this small discrepancy between the expected and measured f_1 is caused by the incident focused laser light from the LDV, which exerts a small optical force gradient on the nanowire. This force gradient can be modeled as an equivalent weak spring ($k_{\text{light}} = 10^{-5}$ N m^{-1}) acting on the end of the nanowire. This spring has the greatest effect on the least stiff eigenmode ($j = 1$), raising the measured first eigenfrequency above that expected.

Measurements of the operating deflection shape (ODS) of NW2 further confirmed the previous identification of the eigenfrequencies from the thermal vibration spectra. For the ODS measurements, NW2 was base excited using a driven excitation mode which allowed the phase of the displacement to be measured (see footnote 8). Figure 2 shows the measured ODS of the second, fourth, sixth, and eighth eigenmodes; movies of the second through eighth ODS are available in the supporting information (available at stacks.iop.org/Nano/21/305701/mmedia). Since k_j increases with eigenmode, the increase in the driven oscillation amplitude, as compared to the thermal motion, is greater for the higher eigenmodes. Taken together, these results indicate that the higher eigenmodes of Ag_2Ga nanowires are accessible and reliably identifiable, thereby suggesting that Ag_2Ga nanowires can be used as well-characterized nanocantilevers in sensing and force transducing applications.

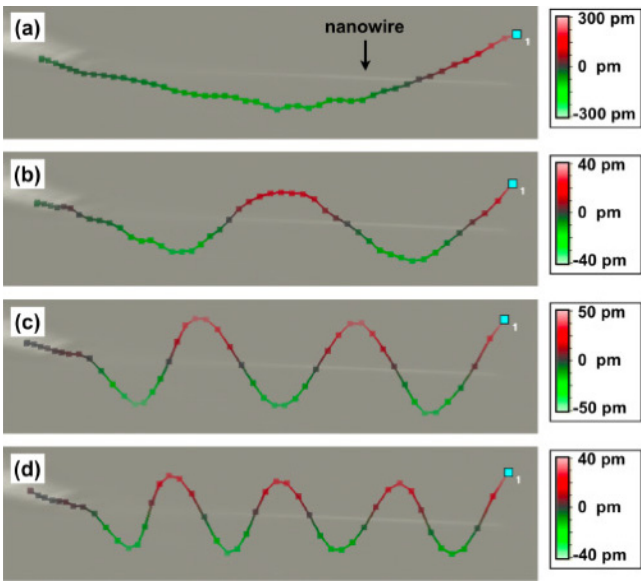

Figure 2. The measured ODS of driven NW2 overlaid on a 50× optical microscope image of NW2. In (a), the 2nd ODS at 0.14 MHz. In (b), the 4th ODS at 0.84 MHz. In (c), the 6th ODS at 2.08 MHz. In (d), the 8th ODS at 3.85 MHz.

4.2. An axially asymmetric Ag_2Ga nanowire with split eigenfrequencies

The measured thermal vibrational spectrum of the Ag_2Ga nanowire NW8 is plotted in figure 3(a). This nanowire was found to have a pair of first eigenfrequency peaks at $f_{1,a} = 0.22$ MHz and $f_{1,b} = 0.46$ MHz and a pair of second eigenfrequency peaks at $f_{2,a} = 1.42$ MHz and $f_{2,b} = 2.79$ MHz. As before, these eigenfrequencies are identified by their ratios, $f_{2,a}/f_{1,a} = 6.40$ and $f_{2,b}/f_{1,b} = 6.03$, both of which are close to the theoretical value of 6.27. Upon closer examination, nanowire NW8 was found to exemplify a non-symmetric nanowire which consists of two parallel conjoined nanowires, 16.6 and 17 μm long, each with a diameter of ∼140 nm, as shown by the SEM micrographs provided in figures 3(b) and (c). The average length of these two nanowires is taken to be $L_{\text{avg}} = 16.8$ μm.

Split eigenfrequency peaks provide a sensitive way to identify the degree of asymmetry in Ag_2Ga nanowires. Circularly symmetric Ag_2Ga nanowires, such as NW2 (see figure 1(b)), have degenerate eigenfrequencies in two orthogonal directions $\hat{x}$ and $\hat{y}$, where $\hat{x}$ and $\hat{y}$ are normal to the long axis of the nanowire. A pair of eigenfrequency peaks, such as seen in figure 3(a), occurs when the areal moment, I,

Table 3. The measured eigenfrequencies and quality factors of Ag_2Ga nanowires NW4 and NW5. Only a single second eigenfrequency above the noise floor was observed for nanowire NW5.

	$f_{1,a}$ (MHz)	$f_{1,b}$ (MHz)	$f_{2,a}$ (MHz)	$f_{2,b}$ (MHz)	$Q_{1,a}$	$Q_{1,b}$	$Q_{2,a}$	$Q_{2,b}$
NW4	2.17	2.44	12.7	14.4	17	28	56	65
NW5	1.18	1.51		8.67	7.4	16		75

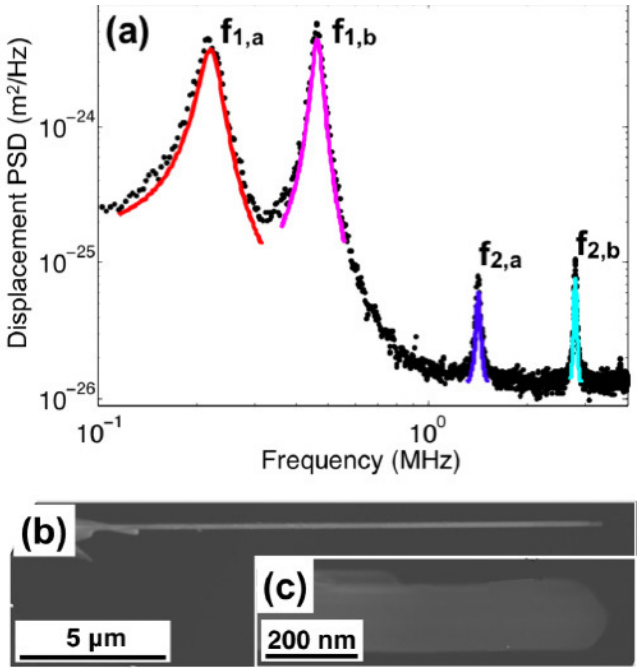

Figure 3. In (a), the thermal vibrational spectrum of asymmetric nanowire NW8 shows two first eigenfrequency peaks at $f_{1,a} = 0.22$ MHz and $f_{1,b} = 0.46$ MHz and two second eigenfrequency peaks at $f_{2,a} = 1.42$ MHz and $f_{2,b} = 2.79$ MHz. In (b) and (c), SEM micrographs of NW8 show two parallel nanowires, 16.6 and 17 μm long.

is no longer degenerate in the $\hat{x}$ and $\hat{y}$ directions. In this case, equation (1) predicts a pair of eigenfrequencies, $\omega_{j,a}$ and $\omega_{j,b}$:

$$\omega_j = \frac{\alpha_j^2}{L^2}\sqrt{\frac{EI}{\rho_L}} \Rightarrow \begin{cases} \omega_{j,a} = \dfrac{\alpha_j^2}{L^2}\sqrt{\dfrac{EI_x}{\rho_L}} \\ \omega_{j,b} = \dfrac{\alpha_j^2}{L^2}\sqrt{\dfrac{EI_y}{\rho_L}}. \end{cases} \tag{10}$$

The large eigenfrequency splitting observed in figure 3 is attributed to the large asymmetry in I. Following equation (10), an estimate of the moment of inertia ratio can be calculated from the ratio of the eigenfrequency pairs,

$$\frac{I_{\hat{y}}}{I_{\hat{x}}} = \left(\frac{\omega_{j,a}}{\omega_{j,b}}\right)^2. \tag{11}$$

For the Ag_2Ga nanowire NW8, the ratio $I_{\hat{y}}/I_{\hat{x}}$ is 0.23 for the first eigenmode and 0.26 for the second eigenmode.

This observation suggests that the cross-sectional area of some nanowires can be better modeled as an ellipse rather than as a circle. The expected ratio of frequency peaks for a nanowire with elliptical cross-section is

$$\frac{\omega_{j,a}}{\omega_{j,b}} = \sqrt{\frac{I_{\hat{y}}}{I_{\hat{x}}}} = \frac{\mathsf{a}}{\mathsf{b}} \simeq 0.5, \tag{12}$$

where a is the semimajor axis and b is the semiminor axis. A value of 0.5 for NW8 can be inferred from the SEM micrographs shown in figure 3. This expectation matches the frequency ratios (0.48 for $j = 1$; 0.51 for $j = 2$) that we measure experimentally.

4.3. The vibrational spectra of short Ag_2Ga nanowires

The vibrational spectra of short ($L < 10$ μm) Ag_2Ga nanowires were studied since the comparatively higher eigenfrequencies of the shorter nanowires lead to a flat frequency response over a wide frequency range. For this reason, the thermal vibration spectra of two short Ag_2Ga nanowires (NW4, ($L = 4.3$ μm, $d_o = 96$ nm) and NW5, ($L = 6.2$ μm, $d_o = 106$ nm)) were measured (figures 4(a) and (b)). Both spectra show a flat frequency response below ~1 MHz. Nanowire NW4 exhibits a pair of split first eigenfrequency peaks at 2.17 and 2.44 MHz; the slightly longer NW5 has a pair of split eigenfrequency peaks at 1.18 and 1.51 MHz (see table 3). For both nanowires, $k_c \sim 0.01$ N m^{-1}.

As described in section 4.2, these split eigenfrequency peaks are attributed to an asymmetrical nanowire cross-section. A close examination of NW5 (figure 4(e)) reveals a second nanowire, only 1.5 μm long, grown parallel to the 6.2 μm long nanowire. From the data listed in table 3 and using equation (12), $\mathsf{a}/\mathsf{b} \simeq 0.78$–$0.89$, indicating that these short Ag_2Ga nanowires may be 'out of round' by 10–25%.

4.4. Q-factors of nanowires at atmospheric pressure

To quantitatively understand the Q-factor of Ag_2Ga nanowires measured under ambient conditions, we note that the measured Q-factor can be written as

$$\frac{1}{Q} = \frac{1}{Q_{\text{gas}}} + \frac{1}{Q_{\text{clamp}}} + \frac{1}{Q_{\text{intrinsic}}}. \tag{13}$$

In equation (13), Q_{gas} accounts for the damping of the oscillating nanowire due to air, Q_{clamp} accounts for the damping due to energy lost at the interface of the nanowire and its support base, and $Q_{\text{intrinsic}}$ represents the energy lost due to intrinsic defects in the nanowire itself.

Since prior studies have shown that Ag_2Ga nanowires are crystalline, for small vibrations, we expect negligible losses due to intrinsic energy loss mechanisms. Since the displacement of the nanowire at the support base is several orders of magnitude smaller than the oscillation amplitude of

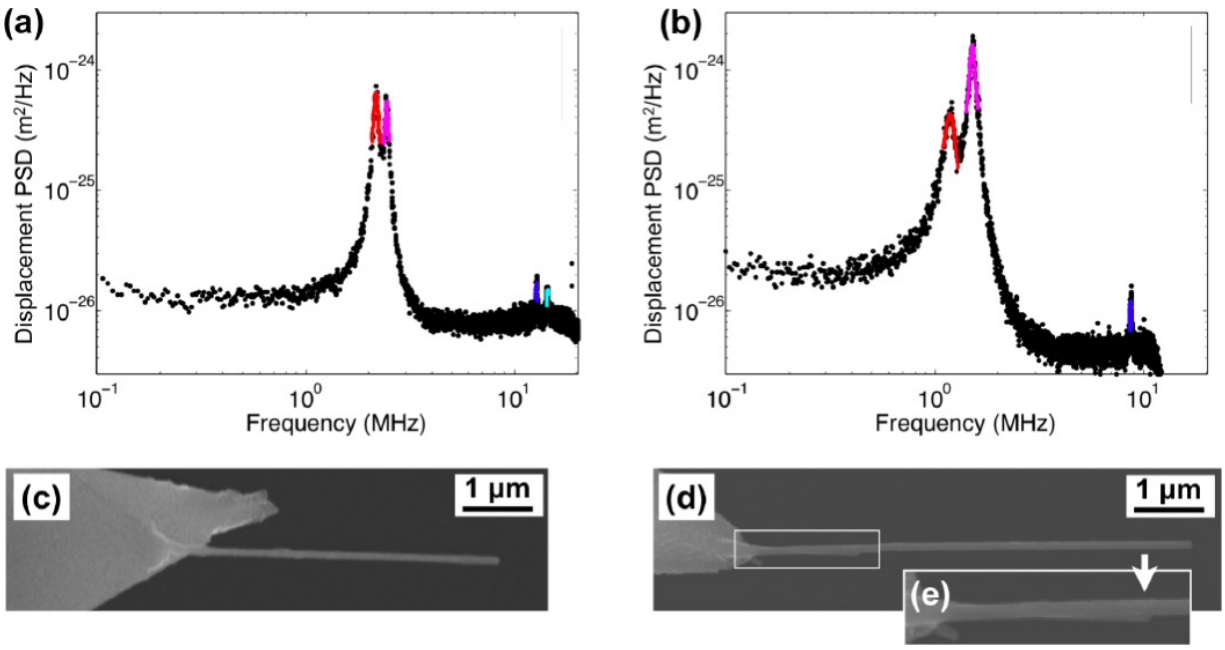

Figure 4. In (a) and (b), log–log plots of the thermal PSDs of NW4 and NW5, respectively, show a flat frequency response below ∼1 MHz. In (c) and (d), SEM micrographs of NW4 and NW5, respectively. An inset (e) shows a second, 1.5 μm long nanowire parallel to NW5.

the free end of the nanowire, we can treat the clamp as a rigid support. We therefore conclude that both $1/Q_{\text{intrinsic}}$ and $1/Q_{\text{clamp}}$ are negligible. For a nanowire vibrating in air, the majority of the energy is dissipated through gas damping in air at ambient pressures.

To further check that gas damping is responsible for the small Q values of Ag_2Ga nanowires, we note that the Knudsen number, $Kn = l_{\text{mfp}}/d$, where l_{mfp}, the mean free path of air molecules, is ∼65 nm for air at STP [24]. The Ag_2Ga nanowires we have studied have $Kn \approx 0.4$, indicating they lie in a cross-over regime ($0.1 < Kn < 10$) [24] for which only approximate gas damping models are available. However at slightly greater Kn numbers ($Kn > 10$), gas damping falls in the free molecular regime and published theories can be used to estimate Q_{gas}. In the free molecular regime, the primary source of damping is momentum transfer due to collisions with the surrounding gas molecules. Assuming a flexible beam and following Christian's model [25] for momentum transfer mediated gas damping in the free molecular regime, we find that an expression for gas damping of the jth eigenmode of the nanowire is given by

$$(Q_{\text{gas}})_j = \frac{\omega_j \rho A}{4bP}\sqrt{\frac{\pi R_o T}{2M_{\text{m}}}}, \qquad (14)$$

where P, R_o, and M_{m}, are the pressure, universal gas constant, and molar mass, respectively. In the case of a cylindrical beam, the effective area for damping per unit length, b, is $\pi d/4$ [26]. From equation (14), we calculate Q_{gas} at atmospheric pressure for Ag_2Ga nanowires of representative diameters. Figure 5 plots the measured Q-factors corresponding to the first eigenmodes of vibration and the calculated Q_{gas}. For the purposes of comparison, we also include representative data for plasma enhanced chemical vapor deposition (PECVD) grown MWNTs [18].

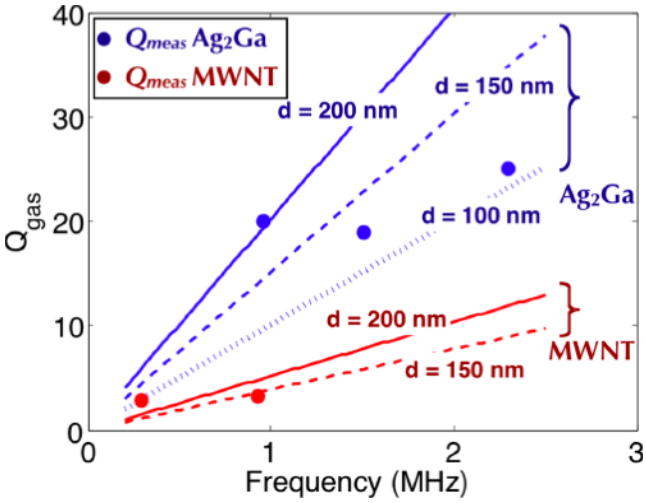

Figure 5. The calculated Q_{gas} for nanowires oscillating at atmospheric pressure, using the calculations of the free molecular flow regime. From equation (14), Q_{gas} is calculated for Ag_2Ga nanowires (blue) and MWNTs (red) of representative diameters. Solid, dashed, and dotted lines correspond to diameters of 200, 150, and 100 nm respectively. Measured Q_{meas}, for Ag_2Ga nanowires and MWNTs ([18]), corresponding to the first eigenmode of vibration, are superimposed on the calculated Q_{gas}.

These calculations of the gas damping confirm that the Q of nanowires oscillating under ambient conditions is dominated by gas damping. Since the density of Ag_2Ga nanowires is approximately three times that of MWNTs ($\rho_{Ag_2Ga} = 8960$ kg m^{-3} versus $\rho_{\text{MWNT}} = 2300$ kg m^{-3}), the Ag_2Ga nanowires have a greater Q at atmospheric pressures.

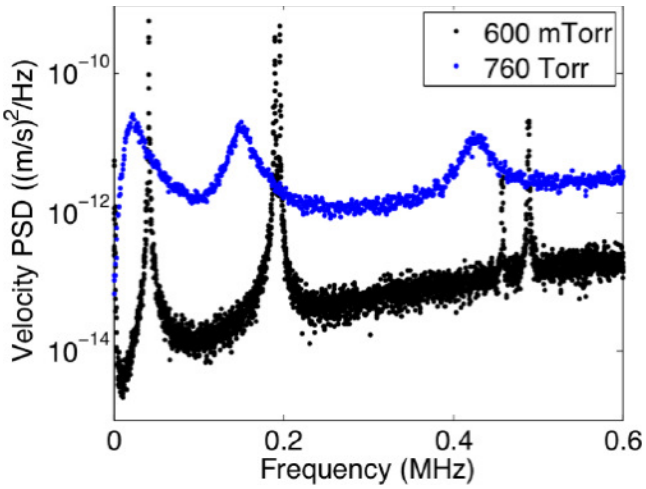

Figure 6. The thermally-excited velocity spectra of nanowire NW2 measured at both 760 Torr and 600 mTorr show the first, second, and third eigenfrequency peaks. Due to the decreased damping at 600 mTorr, the eigenfrequency peaks are shifted to higher frequencies, have higher quality factors, and show a resonant frequency splitting.

5. Vibrations of a Ag_2Ga nanowire measured in low vacuum

The quality factor of a specific eigenmode quantifies how much energy is dissipated during one oscillation cycle. High Q (small energy dissipation) is desirable for many applications. For this reason it is interesting to evaluate the intrinsic Q-factors of Ag_2Ga nanowires at low pressures, to ascertain their intrinsic damping without complications due to gas damping.

After measurement at ambient pressures, one of the Ag_2Ga nanowires (NW2) was mounted in a vacuum chamber and the vibrational spectrum was measured as a function of pressure. The resonant peaks of NW2 sharpened and shifted to higher frequencies due to the elimination of mass loading and viscous damping by the surrounding gas. The quality factors of the oscillations in vacuum ($Q_j \simeq$ 200–600 at 600 mTorr) are two to three orders of magnitude greater than those measured under ambient conditions.

A comparison between the low vacuum and atmospheric thermal vibrational spectrum for nanowire NW2 is illustrated in figure 6. In the 600 mTorr spectrum, the second and third eigenfrequency peaks show a resonant frequency splitting, indicating a slight nanowire asymmetry. The greater damping at 760 Torr masked this splitting. Following the measurements, least squares curve fits using equation (6) were used to accurately determine f_j^{vac} and Q_j^{vac}. The results are summarized in table 4.

Table 4. A comparison of the eigenfrequencies and quality factors of NW2 at 760 Torr (f_j^{atm} and Q_j^{atm}; table 2) and 600 mTorr (f_j^{vac} and Q_j^{vac}), which were measured using the velocity decoder. Split eigenfrequency pairs are observed for f_2^{vac} and f_3^{vac}.

j	f_j^{atm} (MHz)	f_j^{vac} (MHz)	Q_j^{atm}	Q_j^{vac}
1	0.0225	0.0417	1.2	170
2	0.151	0.191, 0.197	6.0	230, 580
3	0.428	0.459, 0.489	12	330, 410
4	0.845	0.787	22	600

6. Discussion

The vibrational properties of Ag_2Ga nanowires have been studied at ambient and low vacuum conditions using LDV techniques. It remains to evaluate the suitability of Ag_2Ga nanowires as resonators for mass sensors and force transducers. For mass sensing applications, resonators with a low mass and a high Q under ambient conditions are desirable [27]. For force transducing applications, a high resonant frequency with a low spring constant is required. In what follows we compare the measured performance specifications of Ag_2Ga nanowires, MWNTs, and typical commercially available Si microcantilevers.

In figure 7(a), we compare the relevant figures of merit for mass sensing applications under ambient pressures (oscillator mass and Q factor under ambient conditions). As shown in figure 7(a), the quality factor of Ag_2Ga nanowires is usually greater than MWNTs of the same diameter. The mass of Ag_2Ga nanowires is 3–5 orders of magnitude smaller than those of typical silicon microcantilevers with only a slightly lower Q factor. The maximum measured Q factor of the Ag_2Ga nanowires is comparable to that of Si microcantilevers (Mikromasch NSC15, width 35 μm, thickness 2 μm).

The minimum detectable mass that can be transduced using each of these resonators has been estimated based on the resulting resonant frequency shift. For the case when an analyte with mass δm binds to a resonator of mass m, the resonance frequency ω_j of the cantilever will be downshifted by an amount $\delta\omega$, where

$$\delta\omega = \frac{\omega_j}{2m}\delta m, \tag{15}$$

assuming the presence of the analyte does not change the stiffness of the cantilever [27, 28]. Assuming that $\delta\omega_{j,\min} = f_j/Q_j$ is the minimum detectable frequency shift yields the minimum detectable masses of $\delta m_{j,\min} = 2m/Q_j$. The minimum detectable mass *under ambient conditions* was found to be in the tens of femtograms range, depending on which of the eight nanowires tested was considered. Under vacuum conditions, the minimum detectable mass usually lies in the attogram range. The fact that many of these nanowires possess split frequencies due to imperfections presents interesting implications for resonant mass and force gradient sensing. For example by tracking frequency shifts in the two split peaks it may become possible to accurately ascertain the exact radial location of the added mass on the nanowire cross-section or the direction of force gradients in two dimensions. A similar sensing idea has been explored using two weakly coupled microcantilevers in which there is a symmetric and antisymmetric mode of oscillation [29].

For force sensing applications the relevant figures of merit are the fundamental natural frequency (the bandwidth of the oscillator) and the inverse of its spring constant (its gain). As shown in figure 7(b), the spring constants of

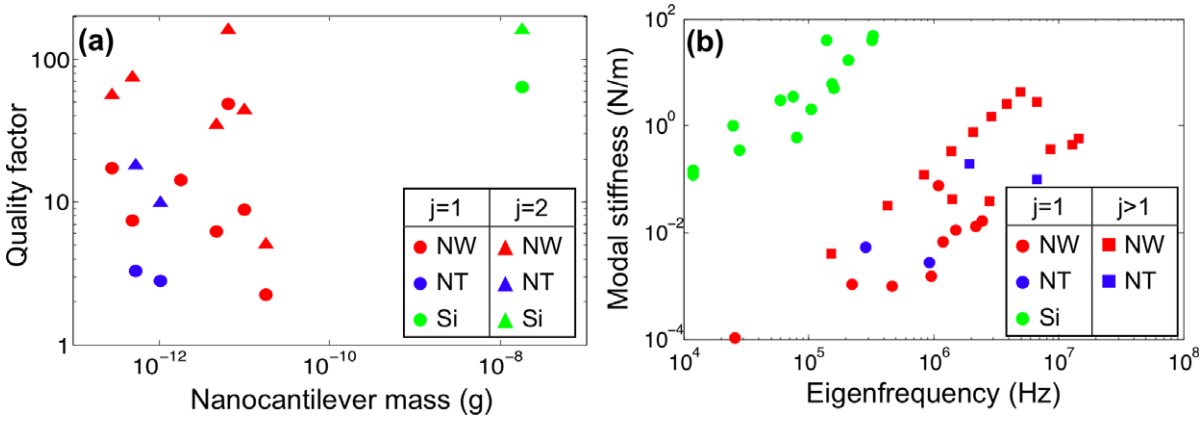

Figure 7. In (a), the measured Q-factors in atmosphere of the first (circles) and second (triangles) eigenmodes of Ag_2Ga nanowires (NW) can be comparable with that of Si microcantilevers (Si) and greater than that of MWNTs (NT). In (b), the stiffness of the first eigenmode (k_1, circles) of Ag_2Ga nanowires is as much as three orders of magnitude less than that of Si microcantilevers. The modal stiffness of the Ag_2Ga nanowires and MWNTs are comparable. Values k_j, f_j, and Q_j for the Ag_2Ga nanowires and MWNTs [18] were experimentally measured; values k_j, f_j, and Q_j of the various Si microcantilevers are the nominal values reported by the manufacturer [30]. Nanocantilever masses were calculated by multiplying the volume of the nanocantilever by its density.

Ag_2Ga nanowires are 2–3 orders of magnitude lower than conventional microcantilevers. The low stiffness and high eigenfrequencies of Ag_2Ga nanowires make them ideal for low force transducing applications. Spring constants on the order of 10^{-2}–10^{-4} N m^{-1} would allow piconewton force detection for nanowire displacements on the order of 1 nm. When considered in this light, Ag_2Ga nanowires can be considered as true nanocantilevers with potential applications in mass sensing and force transduction. For example, Ag_2Ga nanowires with flat frequency responses would be ideal sensing elements for acoustic transducers and accelerometers.

7. Conclusions

We have shown that the optical reflection of light from cantilevered Ag_2Ga nanowires with diameters as small as 65 nm can be used to systematically study the nanowires' vibrational properties using a laser Doppler vibrometer (LDV). From the LDV measurements of the thermal vibration spectra, the elastic modulus (84.4 ± 0.6 GPa) and modal stiffnesses are calculated. We show that crystalline Ag_2Ga nanowires possess many ideal characteristics for nanoscale force transduction and mass sensing, including extremely small spring constants (as low as 10^{-4} N m^{-1}), high frequency bandwidth with resonance frequencies in the 0.02–10 MHz range, small suspended mass (picograms), and relatively high Q-factors ($\sim$2–50) under ambient conditions. These characteristics favor the use of Ag_2Ga nanocantilevers for applications such as femtogram mass sensing and high frequency, piconewton force detection. This study further suggests that Ag_2Ga nanowires may find broad use where novel cantilevers with nanoscale dimensions are desirable, namely as accelerometers, chem-bio mass sensors, atomic force microscope force transducers, and highly sensitive acoustic sensors.

Acknowledgments

The authors acknowledge helpful discussions with S Howell during the course of this work. The Kentucky Science and Technology Corporation supported MY and RC through a Kentucky Commercialization Fund grant and NaugaNeedles LLC through an ICC Concept Pool award. LB was supported by a Purdue Excellence in Science and Engineering Fellowship from Sandia National Laboratories.

References

[1] Fritz J, Baller M K, Lang H P, Rothuizen H, Vettiger P, Meyer E, Guntherodt H J, Gerber C and Gimzewski J K 2000 Translating biomolecular recognition into nanomechanics *Science* **288** 316–8

[2] Wu G H, Datar R H, Hansen K M, Thundat T, Cote R J and Majumdar A 2001 Bioassay of prostate-specific antigen (PSA) using microcantilevers *Nat. Biotechnol.* **19** 856–60

[3] McKendry R *et al* 2002 Multiple label-free biodetection and quantitative DNA-binding assays on a nanomechanical cantilever array *Proc. Natl Acad. Sci. USA* **99** 9783–8

[4] Pinnaduwage L A *et al* 2003 A microsensor for trinitrotoluene vapour *Nature* **425** 474

[5] Arntz Y, Seelig J D, Lang H P, Zhang J, Hunziker P, Ramseyer J P, Meyer E, Hegner M and Gerber C 2003 Label-free protein assay based on a nanomechanical cantilever array *Nanotechnology* **14** 86–90

[6] Waggoner P S and Craighead H G 2007 Micro- and nanomechanical sensors for environmental, chemical, and biological detection *Lab Chip* **7** 1238–55

[7] Ekinci K L, Yang Y T and Roukes M L 2004 Ultimate limits to inertial mass sensing based upon nanoelectromechanical systems *J. Appl. Phys.* **95** 2682–9

[8] Yang Y T, Callegari C, Feng X L, Ekinci K L and Roukes M L 2006 Zeptogram-scale nanomechanical mass sensing *Nano Lett.* **6** 583–6

[9] Jensen K, Kim K and Zettl A 2008 An atomic-resolution nanomechanical mass sensor *Nat. Nanotechnol.* **3** 533–7

[10] Ekinci K L and Roukes M L 2005 Nanoelectromechanical systems *Rev. Sci. Instrum.* **76** 061101

[11] He R R, Feng X L, Roukes M L and Yang P D 2008 Self-transducing silicon nanowire electromechanical systems at room temperature *Nano Lett.* **8** 1756–61

[12] Yazdanpanah M M, Harfenist S A, Safir A and Cohn R W 2005 Selective self-assembly at room temperature of individual freestanding Ag2Ga alloy nanoneedles *J. Appl. Phys.* **98** 073510

[13] Yazdanpanah M M 2006 *PhD Dissertation* University of Louisville
[14] Poncharal P, Wang Z L, Ugarte D and de Heer W A 1999 Electrostatic deflections and electromechanical resonances of carbon nanotubes *Science* **283** 1513–6
[15] Dobrokhotov V V, Yazdanpanah M M, Pabba S, Safir A and Cohn R W 2008 Visual force sensing with flexible nanowire buckling springs *Nanotechnology* **19** 035502
[16] DeBona F and Zelenika S 1997 A generalized elastica-type approach to the analysis of large displacements of spring-strips *J. Mech. Eng. Sci.* **211** 509–17
[17] Yazdanpanah M M, Hosseini M, Pabba S, Berry S M, Dobrokhotov V V, Safir A, Keynton R S and Cohn R W 2008 Micro-wilhelmy and related liquid property measurements using constant-diameter nanoneedle-tipped atomic force microscope probes *Langmuir* **24** 13753–64
[18] Biedermann L B, Tung R C, Raman A and Reifenberger R G 2009 Flexural vibration spectra of carbon nanotubes measured using laser Doppler vibrometry *Nanotechnology* **20** 035702
[19] Nakayama K S, Yokoyama Y, Ono T, Chen M W, Akiyama K, Sakurai T and Inoue A 2010 Controlled formation and mechanical characterization of metallic glassy nanowires *Adv. Mater.* **22** 872–5
[20] Portoles J F, Cumpson P J, Hedley J, Allen S, Williams P M and Tendler S J B 2006 Accurate velocity measurements of AFM-cantilever vibrations by Doppler interferometry *J. Exp. Nanosci.* **1** 51–62
[21] Butt H J and Jaschke M 1995 Calculation of thermal noise in atomic-force microscopy *Nanotechnology* **6** 1–7
[22] Landau L and Lifshitz E M 1984 *Statistical Physics* (Oxford: Butterworth-Heinemann)
[23] Melcher J, Hu S Q and Raman A 2007 Equivalent point-mass models of continuous atomic force microscope probes *Appl. Phys. Lett.* **91** 053101
[24] Bhiladvala R B and Wang Z J 2004 Effect of fluids on the Q factor and resonance frequency of oscillating micrometer and nanometer scale beams *Phys. Rev.* E **69** 036307
[25] Christian R G 1966 Theory of oscillating-vane vacuum gauges *Vacuum* **16** 175–8
[26] Newell W E 1968 Miniaturization of tuning forks *Science* **161** 1320–6
[27] Cleland A N 2005 Thermomechanical noise limits on parametric sensing with nanomechanical resonators *New. J. Phys.* **7** 235
[28] Vignola J F, Judge J A, Jarzynski J, Zalalutdinov M, Houston B H and Baldwin J W 2006 Effect of viscous loss on mechanical resonators designed for mass detection *Appl. Phys. Lett.* **88** 041921
[29] Spletzer M, Raman A, Wu A Q, Xu X and Reifenberger R 2006 Ultrasensitive mass sensing using mode localization in coupled microcantilevers *Appl. Phys. Lett.* **88** 254102
[30] Mikromasch Si cantilevers models SCD14, SCD15, SCD16, SCD17, SCD18, SCD19, NSC11, NSC21, CSC11, and CSC21 were considered www.spmtips.com